Vol 18 No 5, May 2009
1674-1056/2009/18(05)/1877-07

Chinese Physics B

© 2009 Chin. Phys. Soc.
and IOP Publishing Ltd

Mechanism of laser-induced plasma shock wave evolution in air*

Zhao Rui(赵 瑞)[a], Liang Zhong-Cheng(梁忠诚)[a], Han Bing(韩 冰)[b],
Zhang Hong-Chao(张宏超)[b], Xu Rong-Qing(徐荣青)[c],
Lu Jian(陆 建)[b], and Ni Xiao-Wu(倪晓武)[b]†

[a] *Center for Optofluidic Technology, Nanjing University of Posts and Telecommunications, Nanjing* 210003, *China*
[b] *Department of Applied Physics, Nanjing University of Science and Technology, Nanjing* 210094, *China*
[c] *College of Optoelectronic Engineering, Nanjing University of Posts and Telecommunications, Nanjing* 210003, *China*

(Received 25 February 2008; revised manuscript received 3 October 2008)

A theoretical model is proposed to describe the mechanism of laser-induced plasma shock wave evolution in air. To verify the validity of the theoretical model, an optical beam deflection technique is employed to track the plasma shock wave evolution process. The theoretical model and the experimental signals are found to be in good agreement with each other. It is shown that the laser-induced plasma shock wave undergoes formation, increase and decay processes; the increase and the decay processes of the laser-induced plasma shock wave result from the overlapping of the compression wave and the rarefaction wave, respectively. In addition, the laser-induced plasma shock wave speed and pressure distributions, both a function of distance, are presented.

Keywords: laser, shock wave, optical beam deflection
PACC: 4262A, 5235T, 4281W

1. Introduction

When a high-power laser beam is focused onto a solid target, the target absorbs the laser energy, melts, evaporates and then forms plasma at the laser focusing area. The high thermal pressure of the created plasma explodes and drives a shock wave into ambient air.[1,2] The plasma shock wave increases rapidly within the short laser pulse duration and then decays quickly into a local sound wave. Based on the two assumptions that the energy release of the point source is instantaneous and environment pressure can be neglected, the classical shock wave model was developed.[3−6] However, when the shock wave decays to a lower pressure, neglecting the environment pressure is inappropriate. Thus, by taking environment pressure into consideration, the shock wave evolution model was improved.[6−9] Also, in practice, the energy release of the explosion source, which is called the energy-altering shock wave, lasts for a while.[10−12] Having developed the energy-altering shock wave model, Raizer[13,14] first observed the laser-induced plasma shock wave experimentally then calculated the velocity of the expanding wave plate. A lot of experimental methods have been developed to detect the evolution of the shock wave, including the photic-acoustic method,[15,16] the mechanical method,[17,18] the optical beam deflection method,[19,20] interferometry,[21,22] high-speed photography,[23,24] holography,[25,26] etc. In recent years, much attention has been paid to the experimental and theoretical studies of shock wave propagation. The interest originates from the application of the plasma shock wave in physics, chemistry, engineering, biology and medicine.[27−30]

Along with the wider application in laser microsurgery,[31] laser shock cleaning[32] and shock wave lithotripsy,[33] a deeper comprehension of laser-induced shock wave evolution and its associated physical parameters is urgently needed. Unfortunately, due to the complexity of the phenomena involved, the mechanism of laser-induced plasma shock wave evolu-

*Project supported by the National Natural Science Foundation of China (Grant Nos 60578015, 60778007 and 60878037), the Natural Science Foundation of the Jiangsu Higher Education Institutions of China (Grant No 05KTB510028), the Scientific Research Starting Foundation for Returned Scholars, Nanjing University of Posts & Telecommunications, China (Grant Nos NY207030 and NY206076).
†Corresponding author. E-mail: nxwhome@mail.njust.edu.cn

tion is little studied.

In the present work, based on the theoretical work in Refs.[12–16], a 'compression-rarefaction-wave' theoretical model is developed to depict the mechanism of plasma shock wave evolution generated during Nd:YAG laser heating of an aluminium target. Experimentally, the evolution of the plasma shock wave is monitored by a well-designed optical fibre sensor based on detecting the beam deflection. As expected, the non-invasive beam-deflection probe succeeds in reproducing laser-induced plasma shock wave evolution, and the good agreement between the theoretical model and the experimental signals confirms the validity of the theoretical model. Experimental data of the shock wave speed and pressure distributions as a function of distance are provided in the present paper. In addition, a numerical calculation is carried out for analytic expressions and the calculations are compared with the measurements.

2. Experimental details

The experimental arrangement is outlined in Fig.1. The Q-switched Nd:YAG laser-delivered pulse of 100 mJ in 10 ns at a wavelength of 1.06 μm is focused onto an aluminium plane target, which is mounted on a four-dimensional regulating platform with a 5-μm spatial resolution. For each test we move the aluminium plane target down and up to ensure experimental precision and prevent the laser-irradiated target point from being eroded by the laser. A group of attenuators are used to adjust the incident laser energy with its spatial distribution kept unchanged. The focal spot on the target is about 100 μm in radius, thus the power density at the spot can reach up to 3.2×10^{10} W/cm^2, which is much higher than the aluminium plasma ignition threshold of 7.5×10^{7} W/cm^2.

In the detection region, the probe beam emitted by a He–Ne laser (power 5 mW, wavelength 0.63 μm) is employed to monitor the laser-induced plasma shock wave evolution process. The reflected beam is focused with a microscope objective onto a single-mode optical fibre mounted on a five-dimensional fibre-regulating stand with a 0.1-μm spatial resolution. Then the light from the optical fibre is fed into a photomultiplier and recorded by a digital oscilloscope (Tektronix TDS340, 1 Gigasample/s). In order to increase the signal-to-noise ratio, a narrow-band interference filter with a central wavelength 0.63 μm is located between the microscope objective and the fibre. The scattered light from a laser pulse is monitored, with a photoelectric diode with 0.1-ns rise time triggered. Here, the experimental parts numbered 7 to 12 in Fig.1 constitute a subsystem, which is called the optical beam deflection (OBD) test system, numbered 16. This OBD part is placed on a two-dimensional platform, which can be moved in the arrowed directions with a spatial resolution of 10 μm, as shown in Fig.1. A detailed description of the detection principle and the setup was reported in our previous paper.[34]

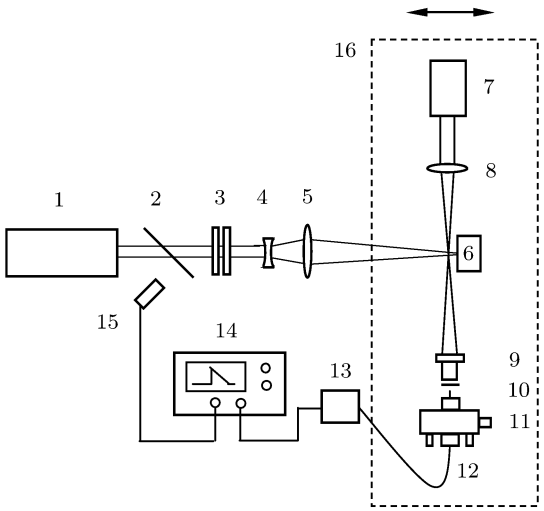


Fig.1. Schematic diagram of experimental setup composed of optical beam deflection 1, Q-switched Nd:YAG 2, beam splitter 3, attenuator group 4, concave lens 5, convex lens 6, aluminium target 7, He–Ne laser 8, convex lens 9, microscope objective (20×, L2, f_2 = 4 mm) 10, interference filter photomultipler (Hamamatsu H5773 with 2ns rise time) 11, 5-axis fibre-regulating-stand 12, single-mode optical fibre PIN photodiode (with 0.1ns rise time) 13, photomultiplier 14, digital oscilloscope (Tektronix TDS340) 15, and PIN photodiode (with 0.1 ns rise time), and 16 optical beam deflection (OBD) test system.

3. Theoretical model of plasma shock wave evolution

3.1. Description of the theoretical model

The planar aluminium target is irradiated by a laser pulse with intensity I_0 and duration τ. The pressure of the laser-induced plasma shock wave is considered to be approximately trapezoidal in profile as shown in Fig.2.

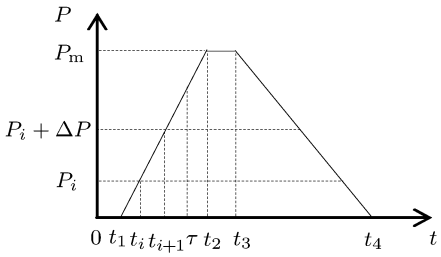


Fig.2. Variation of the plasma shock wave pressure.

From $t = 0$ to t_1, when the laser pulse reaches an energy intensity larger than the breakdown threshold of the aluminium target, a small portion of the aluminium target in the laser focal area begins to melt and evaporate. Continuous heating and ablation of target material lead to plasma generation. The high thermal pressure plasma expands, and drives a hemispherical shock wave at speed U into ambient air of the target at time t_1.

During the time$t_1 < t < \tau$, the laser-induced plasma shock wave propagates into the air at speed U, and imparts a speed u to the air behind the shock wave front. Before the laser pulse terminates, a portion of the ablated material absorbs the subsequent laser energy, thereby creating a powerful compression wave. The compression wave travels at a speed of $C + u$, which is higher than the spherical shock wave speed U, thus the compression wave eventually catches up with the spherical shock wave and leads to a direct increase in the amplitude of the spherical shock wave pressure. It is found that the compression wave continues to propagate and the amplitude of the plasma shock wave pressure is on the increase when the laser pulse terminates until the compression wave overlaps the plasma shock wave at $t = t_2$. As expected, due to the termination of the laser pulse, the ablated material vapour pulse begins to drop off rapidly at time $t = \tau$. Once the ablation material wave vanishes, a rarefaction wave emerges and travels into the spherical shock wave. Since the leading edge of the rarefaction wave also travels at a speed of $C+u(C+u > U)$, the rarefaction wave will overtake the spherical shock-wave front at time t_3 and begin to whittle it down. Therefore, the plasma shock wave stays in the steady propagation stage in the time interval $t_2 < t < t_3$. It attenuates drastically during the time $t_3 < t < t_4$ and eventually decays into an acoustic wave at time t_4.

3.2. Equations of the theoretical model

Considering a discontinuous shock wave front and an isentropic flow, the conservation of mass and momentum equations, with only one space variable x (i.e. in the arrowed direction as shown in Fig.1), give expressions for the shock evolution as follows:[35]

$$\frac{\partial u}{\partial t} + u\frac{\partial u}{\partial x} + \frac{1}{\rho}\frac{\partial p}{\partial x} = 0, \tag{1}$$

$$\frac{\partial p}{\partial t} + u\frac{\partial p}{\partial x} + \rho C^2\frac{\partial u}{\partial x} = 0. \tag{2}$$

The Hugoniot sound speed behind the shock wave front is determined by

$$C^2 = \frac{\mathrm{d}p}{\mathrm{d}\rho}. \tag{3}$$

The analytic expression for the Hugoniot sound speed behind the shock wave front is expressed as[36]

$$C = v \cdot \left\{ \frac{2(\gamma-1)}{(\gamma+1)^2}\left[\gamma\left(\frac{U}{v}\right)^2 - \left(\frac{v}{U}\right)^2\right] + \frac{8\gamma}{(\gamma+1)^2} - 1 \right\}^{1/2}, \tag{4}$$

where C is the Hugoniot sound speed; U and v are the shock wave speed and the sound speed at ambient temperature; γ is the ratio of specific heats.

Neglecting the shock wave reflection, the relationship at the shock wave front is shown as follows:

$$\frac{\mathrm{d}p}{\mathrm{d}x} = \frac{\partial p}{\partial x} + \frac{1}{U}\frac{\partial p}{\partial t}, \tag{5}$$

where x is the shock front position, $\mathrm{d}p/\mathrm{d}x$ is the variation of shock amplitude, $\partial p/\partial x$ is the pressure gradient immediately behind the shock front, and ρ is the material density.

Since the particle speed u is a function of x and t, we obtain

$$\frac{\mathrm{d}u}{\mathrm{d}x} = \frac{\partial u}{\partial x} + \frac{1}{U}\frac{\partial u}{\partial t}. \tag{6}$$

Equation (6) can also be written as

$$\frac{\partial u}{\partial t} = U\left(\frac{\mathrm{d}u}{\mathrm{d}x} - \frac{\partial u}{\partial x}\right). \tag{7}$$

From Eqs.(1), (2) and (7) it follows that

$$\frac{\partial p}{\partial t} + \left(u + \frac{C^2}{U-u}\right)\frac{\partial p}{\partial x} + \frac{\rho_0 U^2 C^2}{(U-u)^2}\frac{\mathrm{d}u}{\mathrm{d}x} = 0. \tag{8}$$

Substituting the following equations $\dfrac{\mathrm{d}u}{\mathrm{d}x} = \dfrac{\mathrm{d}u}{\mathrm{d}P}\dfrac{\mathrm{d}p}{\mathrm{d}x}$ and $\dfrac{\partial p}{\partial x} = \dfrac{\mathrm{d}p}{\mathrm{d}x} - \dfrac{1}{U}\dfrac{\partial P}{\partial t}$ into Eq.(8) yields

$$\frac{\mathrm{d}p}{\mathrm{d}x} = \frac{\left[C^2 - (U-u)^2\right]\dfrac{\partial p}{\partial t}}{U\left[C^2 + u(U-u)\right] + \dfrac{\rho_0 C^2 U^3}{U-u}\dfrac{\mathrm{d}u}{\mathrm{d}p}}. \tag{9}$$

In Eq.(9), the term $\mathrm{d}u/\mathrm{d}p$ can be calculated below.

From the Rankine–Hugoniot equation, the instantaneous pressure behind the shock wave front is given as[36]

$$p = \frac{2}{\gamma+1}\rho_0 U^2 - \frac{\gamma-1}{\gamma+1}p_0, \tag{10}$$

where p is the pressure immediately behind the shock front, p_0 is the atmospheric pressure in front of the shock wave, U is the shock wave speed, and γ is the ratio of specific heats.

The shock wave speed U and the particle speed u are linearly related to a first approximation

$$U = C_0 + Su, \tag{11}$$

where u is the particle speed, $C_0 = 0.899\,\mathrm{km/s}$, and $S = 0.939$ in air.[37]

Using expressions (10) and (11), the differential expression $\mathrm{d}u/\mathrm{d}p$ is described as

$$\frac{\mathrm{d}u}{\mathrm{d}p} = \frac{\gamma+1}{4\rho_0 SU}. \tag{12}$$

Now we follow Cotett and Romain[38] to calculate the term $\partial p/\partial t$ in Eq.(9).

Assuming that the spherical shock wave amplitude is p_i at time t_i and distance x_i (Fig.2), a compression wave at speed $C+u$ overtakes the spherical shock wave at x_i and leads to a direct increase in the amplitude of the spherical shock wave $p_i + \Delta p$ at time t_{i+1}. The $\partial p/\partial t$ can be deduced by the limit of $\Delta p/\Delta t$ as $\Delta p \to 0$. A similar expression can also be derived for the spherical shock wave decay process. The general expression $\partial p/\partial t$ for both increase and decay of the spherical shock wave is given as follows:

$$\begin{aligned}\frac{\partial p}{\partial t} &= \lim_{\Delta p\to 0}\left.\frac{(p_i+\Delta p)-p_i}{t_{i+1}-t_i}\right|_{x_i} \\ &= (-1)^{n+1}\left[\frac{\tau}{p_m} + (-1)^n \frac{x}{(C+u)^2}\left(\frac{\mathrm{d}u}{\mathrm{d}p} + \frac{\mathrm{d}C}{\mathrm{d}p}\right)\right]^{-1} \\ &= (-1)^{n+1}\left[\frac{\tau}{p_m} + (-1)^n \frac{x}{(C+u)^2}\left(\frac{1}{\rho_0(2U-C_0)} + \frac{(\gamma-1)(U-u)}{2\rho_0 CU}\right)\right]^{-1},\end{aligned} \tag{13}$$

where τ is the laser pulse duration, p_m is the maximum pressure of the spherical shock wave, $n=1$ is for the case of spherical shock wave increase, while $n=2$ is for the case of spherical shock wave decay.

Substituting Eqs.(12) and (13) into Eq.(9) yields

$$\begin{aligned}\frac{\mathrm{d}p}{\mathrm{d}x} = &\frac{(-1)^{n+1}}{U\left[C^2+u(U-u)\right] + \dfrac{C^2U^3}{(U-u)(2U-C_0)}} \\ &\times \frac{\left[C^2-(U-u)^2\right]}{\frac{\tau}{p_\mathrm{m}} + (-1)^n \dfrac{x}{(C+u)^2}\left[\dfrac{1}{\rho_0(2U-C_0)} + \dfrac{(\gamma-1)(U-u)}{2\rho_0 CU}\right]}.\end{aligned} \tag{14}$$

It is worth noting that Eqs.(13) and (14) are applicable only to spherical geometry.

4. Results and discussion

Experimentally, the evolution of the plasma shock wave generated by a Q-switched Nd:YAG laser irradiating a target is tracked by a well-designed optical fibre sensor based on the detection of beam deflection. Figure 3 shows a series of typical deflection signals of the laser-induced plasma shock wave formation and propagation processes monitored at different positions away from the target surface. In Fig.3, indices 1–5 denote the plasma shock wave, the compression wave, the ablated material vapour pulse, the rarefaction wave and the acoustic transient, respectively. To eliminate random errors, the experimental data collected in this paper are the average values over five measurements.

When a laser pulse with a power density above

the aluminium breakdown threshold is focused on the target surface, it causes explosive vaporization of the surface material. The ablated material vapour pulse expands away from the surface at a considerable speed and is indicated as peak a_3 in Fig.3(a).

Continuous heating leads to electron avalanche breakdown, thereby turning part of the ablated material into a high-temperature, high-pressure plasma state. The high thermal pressure plasma expands and drives a spherical shock wave into the air. We refer to this spherical shock wave as a laser-induced plasma shock wave, which is indicated as peak b_1 in Fig.3(b). From Fig.3(b), it can be seen that the laser-induced plasma shock wave detected at 0.85 mm away from the target cannot be easily distinguished from the vapour pulse b_3 at distances less than the above distance.

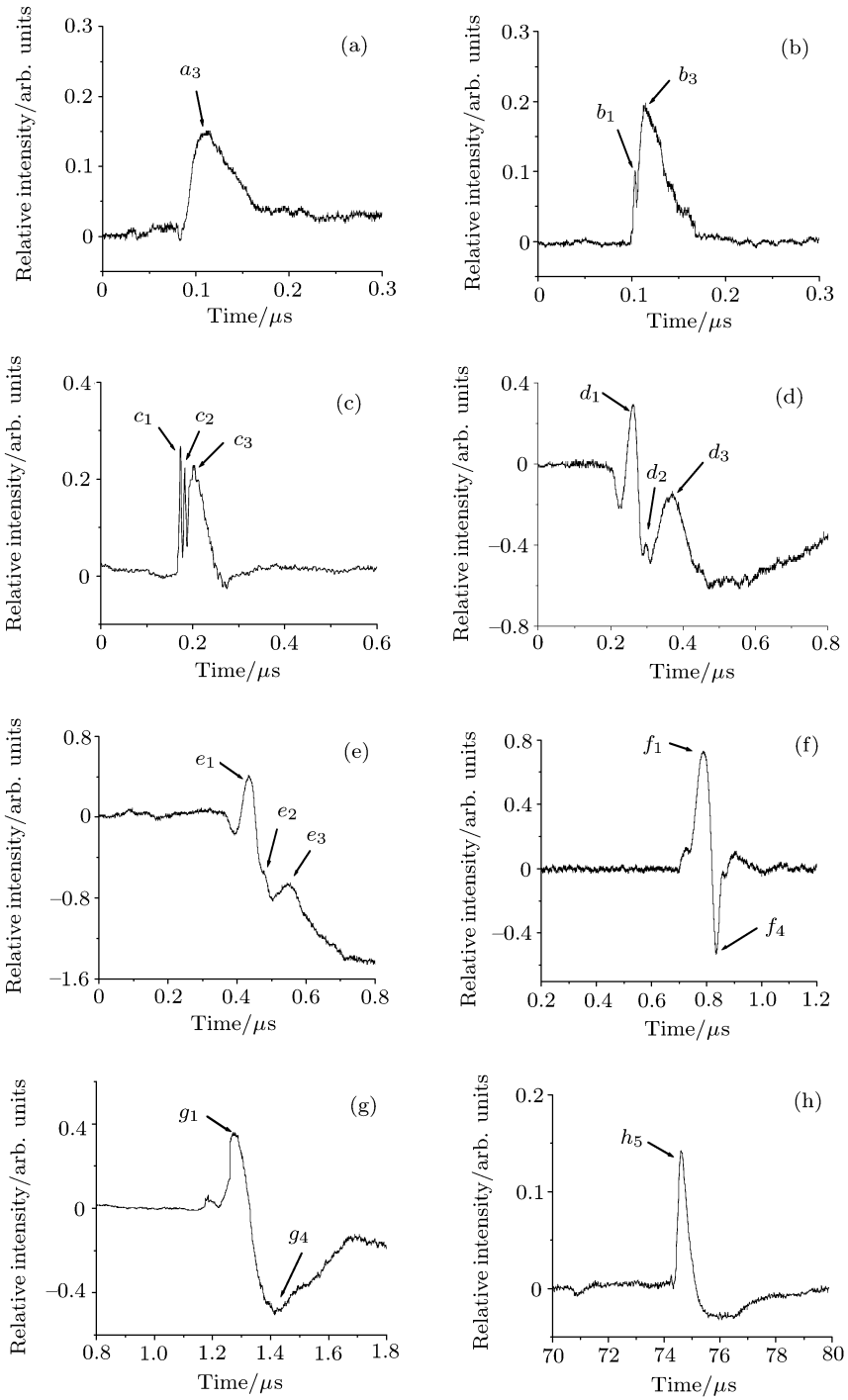


Fig.3. Typical deflection signals of laser-induced plasma shock wave formation and propagation processes detected at different positions: (a) 0.52 mm, (b) 0.85 mm, (c) 0.94 mm, (d) 1.1 mm, (e) 1.54 mm, (f) 2.68 mm, (g) 3.55 mm, and (h) 30 mm.

In the following stage, the ablated materials absorb the subsequent laser energy continuously and partly form a powerful thermal wave. This powerful thermal wave acts as a compression wave and enters into the air, which is indicated as peak c_2 in Fig.3. Since the compression wave behind the shock wave front travels at a higher speed than the plasma shock wave, it rapidly catches up with and eventually overlaps the plasma shock wave at 2.68 mm away from the target after propagating for 0.84 μs. It can be seen from Figs.3(c)–3(f) that the amplitude of the compression wave, namely peak 2, becomes smaller and eventually disappears, while the plasma shock wave becomes stronger and reaches its maximum value.

When the laser pulse terminates, the ablated material vapour indicated as peak 3 in Fig.3 begins to drop and disappears at about 2.68 mm due to tremendous energy dissipation. Once the ablated material pulse vanishes, a rarefaction wave comes into being and propagates into the air towards the plasma shock wave at a higher speed. The rarefaction wave leads to a downward negative peak deflection signal and is denoted as peak 4 in Fig.3(f), which is also reported in Refs.[39, 40]. When the rarefaction wave overtakes the plasma shock wave, the rarefaction wave attenuates the shock wave rapidly due to its stronger pull effect. Accordingly, the plasma shock wave becomes lower and wider until it decays into an acoustic wave. On the other hand, the rarefaction wave changes into a weaker sparse wave and vanishes in succession, which is shown in Fig.3(f)–3(h). As expected, the beam deflection signals succeed in depicting the evolution of the laser-induced plasma shock wave and demonstrate the validity of the theoretical model mentioned previously. It indicates that the laser-induced plasma shock wave undergoes formation, increase and decay stages, which agrees well with the results obtained in other research studies.[2,39,40] Moreover, we consider that the increase and decay processes of the shock wave result from the chase effect of the compression wave and rarefaction wave, respectively.

By tracking the time for the laser-induced plasma shock wave to arrive at the corresponding detection distance, the plasma shock wave speed distribution as a function of distance can be obtained, which is shown in Fig.4. The experimental result indicates that the plasma shock wave speed increases quickly to a maximum value of 2.29 km/s at 2.68 mm away from the target surface, and then decreases exponentially to 550 m/s within a distance of about 6.5 mm from the emission centre. Afterwards the plasma shock wave propagates forward into the air with slowly and almost linearly decreasing speed till it decays into an acoustic wave at about 30 mm away. It should be noted that the results are consistent with other results.[41,42]

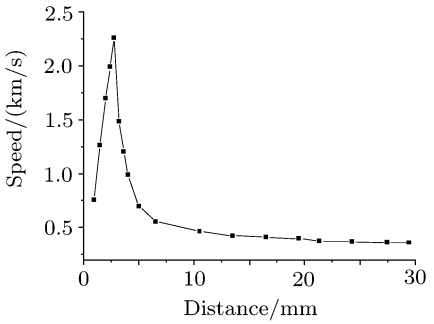


Fig.4. Distance-dependent speed velocities of the plasma shock wave.

As the speed of the laser-induced plasma shock wave is known, the experimental shock wave pressure distribution as a function of distance can be calculated from expression (10). The numerical calculation of the shock wave pressure distribution $p(x)$ can also be carried out by using the analytical expression (14) and then the numerical results are compared with the experimental results. Both the experimental results and the numerical results are plotted in Fig.5. It is evident that they are in fairly good agreement with each other within a relatively small error. The pressure of the laser-induced plasma shock wave increases much faster from the ambient pressure of 1 atm to a maximum value of 5.60 MPa in a 2.68 mm range; in the region where $x > 2.68$ mm, the pressure decreases much faster in the near field than in the far field, i.e. the exponential decay process varying according to the nonlinearity law holds true. Similar results have been obtained in Refs.[43, 44].

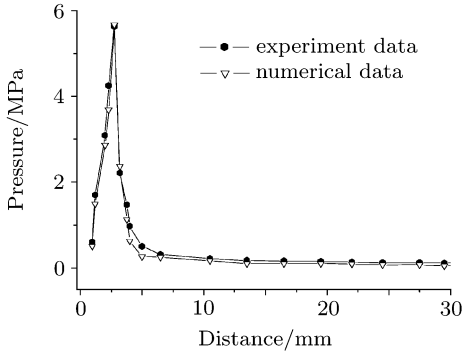


Fig.5. Spatial distribution of the plasma shock wave pressure.

5. Conclusions

In this paper, the evolution of a laser-induced plasma shock wave in air is investigated using a theoretical model. Also, it is monitored by a highly sensitive fibre-optic sensor based on the optical beam deflection technique. The non-invasive probe reproduces the characteristics of laser-induced plasma shock wave evolution and provides experimental data of the shock wave speed and pressure distributions as a function of distance. The theoretical model developed in this work confirms these results well, implying that the theoretical model is a good approximation to the description of plasma shock wave evolution. The laser-induced plasma shock wave undergoes formation, increase and decay processes. The increase results from the chasing effect of the compression wave, and the decay is induced by the pulling effect of the rarefaction wave.

The results presented here will help further research into the mechanism of laser-induced plasma shock wave evolution and enrich the application of laser-induced plasma shock waves.

References

[1] Zeng X Z, Mao X L, Mao S S, Wen S B, Greif R and Russo R E 2006 *Appl. Phys. Lett.* **88** 061502
[2] Guo H P, Lou Q H, Chen S C, Cheung N H, Wang Z Y and Lin P K 1993 *Opt. Commun.* **98** 220
[3] Taylor G I 1950 *Proceedings Soyal Society* A **201** 175
[4] Sakurai A in Holt M (editors) 1965 *Basic Developments in Fluid Dynamics* (New York: Academic Press) p309
[5] von Neumann J 1963 *The Point Source Solution, Collected Works* (Oxford: Pergamon) **6** 219
[6] Bach G G and Lee J H 1970 *AIAA* **8** 271
[7] Oshima K 1964 *Aeronautical Research Institute University of Tokyo Report* p386
[8] Jones D L 1968 *Physics of Fluids* **11** 1664
[9] Chen X, Bian B M, Shen Z H, Lu J and Ni X W 2003 *Microwave and Optical Technology Letters* **38** 75
[10] Freeman R A 1968 *J. Appl. Phys.* D **1** 1697
[11] Dabora E K 1972 *AIAA J.* **10** 1384
[12] Director M N 1977 *AIAA J.* **15** 1315
[13] Raizer Y P 1965 *Soviet Physics JETP* **21** 1009
[14] Raizer Y P 1965 *Zho lksp Teor. Fiz.* **48** 1508
[15] Stephen A 1993 *SPIE* **1882** 1321
[16] Vogel A 1999 *Appl. Phys.* B **68** 271
[17] Schoeffmann H, Schmidt K H and Reichel E 1988 *J. Appl. Phys.* **63** 46
[18] Vogel A, Lauterborn W and Timm R 1989 *J. Fluid Mech.* **206** 299
[19] Doukas A G, Zweig A D, Frisoli J K, Birngruber R and Deutsch T F 1991 *Appl. Phys.* B **53** 237
[20] Chen J P, Ni X W, Lu J, Bian B M and Wang Y W 2000 *Microwave and Optical Technology Letters* **25** 307
[21] Gidon S and Behar G 1986 *Appl. Optic.* **25** 1429
[22] Ni X W, Lu J and He A Z 1997 *Microwave and Optical Technology Letters* **14** 271
[23] Schiffers W P, Shaw S J and Emmony D C 1998 *Ultrasonics* **36** 559
[24] Shaw S J, Schiffers W P and Emmony D C 2001 *J. Acoust. Soc. Am.* **110** 1822
[25] Harith M A, Palleschi V, Salvetti A, Singh D P, Tropiano G and Vaselli M 1989 *Opt. Commun.* **71** 76
[26] Gatti M, Palleschi V, Salvetti A, Singh D P and Vaselli M 1988 *Opt. Commun.* **69** 141
[27] van Capel P J S and Dijkhuis J I 2006 *Appl. Phys. Lett.* **88** 151910
[28] Azzeer A M, Al-Dwayyan A S, Al-Salhi M S, Kamal A M and Harith M A 1996 *Appl. Phys.* B **63** 307
[29] Petkovšek R, Možina J and Močnik G 2005 *Opt. Express* **13** 4107
[30] Koenig M, Benuzzi-Mounaix A, Philippe F, Faral B, Batani D, Hall T A, Grandjouan N, Nazarov W, Chieze J P and Teyssier R 1999 *Appl. Phys. Lett.* **75** 3026
[31] Glezer E N, Schaffer C B, Nishimura N and Mazur E 1997 *Opt. Lett.* **22** 1817
[32] Lim H and Kim D 2004 *Appl. Phys.* A: *Mater. Sci. Process* A **79** 965
[33] Chitnis P V and Cleveland R O 2006 *J. Acoust. Soc. Am.* **119** 1929
[34] Chen J P, Ni X W, Lu J and Bian B M 1999 *Opt. Commun.* **168** 343
[35] Lü H S and Zeng X W 1999 *Hydromechanics and Blast Mechanics* (National University of Defense Technology Press) p122 (in Chinese)
[36] Li W X 2003 *One-dimensional Nonsteady Flow and Shock Waves* (National Defence Industry Press) p209, p218 (in Chinese)
[37] Cooper P W 1996 *Explosives Engineering* (New York: VCH Publisher IR) p189
[38] Cottet F and Romain J P 1982 *Phys. Rev.* A **25** 576
[39] Attenborough K and Qin Q 2002/2003 *Central Laser Facility Annual Report* p159
[40] Koren G 1987 *Appl. Phys. Lett.* **51** 569
[41] Márton Zs, Heszler P, Mechler Á, Hopp B, Kántor Z and Bor Zs 1999 *Appl. Phys.* A **69** 133
[42] Lackner M, Charareh S, Winter F, Iskra K F, Rüdisser D and Neger T 2004 *Opt. Express* **12** 4546
[43] Bian B M, He F, Chen J P, Ni X W and Lu J 2001 *Chin. J. Lasers* A **28** 155 (in Chinese)
[44] Chumakov A M, Petrenko A M and Bosak N A 2002 *Journal of Engineering Physics and Thermophysics* **75** 725